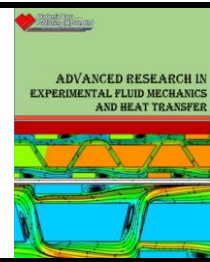




Journal of Advanced Research in Experimental Fluid Mechanics and Heat Transfer

<http://www.akademiabaru.com/submit/index.php/arefmht>

ISSN: 2756-8202



Open
Access

Experimental and Numerical Study on the Effect of Teardrop Dimple/Protrusion Spacing on Flow Structure and Heat Transfer Characteristics

Ye Min Oo¹, Makatar Wae-hayee^{1,2,*}, Chayut Nuntadusit^{1,2}

¹ Department of Mechanical Engineering, Faculty of Engineering, Prince of Songkla University, Hatyai, 90112 Songkhla, Thailand

² Energy Technology Research Centre, Faculty of Engineering, Faculty of Engineering, Prince of Songkla University, Hatyai, 90112 Songkhla, Thailand

ABSTRACT

In this study, the flow characteristics and heat transfer were analyzed in rectangular wind tunnel installed with the teardrop dimples and protrusions. The flow characteristics, spacing effect on the heat transfer enhancement, Turbulence Kinetic Energy (TKE) and thermal performance are the main objectives of this study under the constant Reynolds number 20,000. The projected diameter of dimple and protrusion was fixed with $D=26.4$ mm and the depth of dimples and protrusions was 5.28 mm ($H=0.2D$). The spacing between protrusion-to-protrusion and dimple-to-dimple was varied with four spacing cases i.e., $S=1.125, 1.25, 1.5$ and $2 D$. The computational fluid dynamics (CFD) was applied for simulation results. In the experimental results, the temperature of protruded surface covering with Thermochromic Liquid Crystal sheet (TLCs) was measured and converted into heat transfer coefficient. The results show that the heat transfer enhancement for teardrop dimple cases is higher than that for protrusion for both experimental and simulation results. When the spacing is getting larger, the thermal performance values for teardrop dimple cases gradually decrease while the values for teardrop protrusion cases gradually increase.

Keywords:

heat transfer, teardrop dimples and protrusions, flow characteristics

Copyright © 2020 PENERBIT AKADEMIABARU - All rights reserved

Received: 12 October 2020

Revised: 1 December 2020

Accepted: 24 January 2021

Published: 2 February 2021

1. Introduction

Heat transfer enhancement techniques are very attracted in various applications of engineering such as internal cooling for turbine air foil, electric cooling devices, heat exchanger and gas turbine blade to solve and save the thermal energy consumption. One of heat transfer enhancement techniques is passive heat transfer enhancement techniques such as ribs, pin fins, dimples, protrusion, and other vortex generators. Among them, the technique using with dimples and protrusions is the most attractive method because it can increase the flow turbulence intensity, which causes heat transfer enhancement. The main function of this technique is to enhance heat transfer convection by reducing or destroying the thermal boundary layer [1]. Many researchers have been carried out the analysis of dimples and protrusions geometries with many applications.

* Corresponding author.

E-mail address: wmakatar@eng.psu.ac.th

The heat transfer enhancement comparison of hemispherical and teardrop dimpled surface with staggered array using transient liquid crystal imaging system was experimentally analysed by Chyu *et al.* [2]. The Reynolds numbers based on the hydraulic diameter were arranged between 10,000 and 52,000. They found that the heat transfer rate for hemispherical and teardrop dimpled cases was increased about 17% and 22% comparing with smooth surface. For the issue of pressure drop, teardrop dimple case was the highest-pressure loss and, both cases were lower pressure penalty than other techniques such as rib turbulators and pin fins.

Relation between flow structure and local heat transfer characteristics over the dimpled surface was studied by Mahmood *et al.* [3]. Low Nusselt number region was found at the upstream half of dimples. The high Nusselt number was occurred at the downstream half of dimples. The highest values were found at just downstream of rims of dimples and smooth surface which is closed to the downstream of dimples because the vortex pair and vortical pair were ejected at those regions.

Ligrani *et al.* [4] studied the effect of channel height to dimple printed diameter (the ratio of channel height to dimple printed diameter ratio H/D were 0.25, 0.5 and 1). The Reynolds number varied from 600 to 11,000 and the ratio of depth to printed diameter of dimple was 0.2. The results of $H/D=1$ was showed that the primary and secondary vortices pairs became strong and lengthened. Moreover, the mixing intensity of smoke patterns and the vortices with streamwise development became stretched.

Recently, Xie *et al.* [5] considered numerically flow and heat transfer characteristics of teardrop dimple and protrusion with positive and negative eccentricity (PE and NE) and compared with hemispherical dimple and protrusion by using CFD technique which is very popular to study flow and heat transfer properties. They used realizable k- ω turbulent model and arranged Reynolds number from 7,000 to 9,000. Their results showed the thermal performance of teardrop dimple was low at $e/D_h=0.1$. However, the thermal performance of teardrop dimple/protrusion was the highest at $e/D_h=0.4$. They concluded that the thermal performance of teardrop dimple/protrusion was good at lower Reynolds number.

Acharya *et al.* [6] studied experimentally and numerically on heat/mass transfer and flow structure for four dimple shapes which were (1) square, (2) triangular, (3) circular, and (4) teardrop in square internal passage at Reynolds number of 21,000. They used naphthalene sublimation method. Their results suggested that the teardrop dimple was the highest heat transfer for both experimental and computational results compared to other shapes.

Furthermore, Rao *et al.* [7] presented the effect of different dimple shapes which were spherical, teardrop, elliptical, and inclined elliptical on the heat transfer and flow structures. All dimples have same depth, and the Reynolds numbers were set the range between 8500 and 60,000. Their study showed that the heat transfer for teardrop dimple was the highest and the spherical dimple was the second highest model. The lowest heat transfer was found in elliptical model. Different shapes of dimple can cause different heat transfer convection and different vortex flow structures.

A study was described numerically the analyzing of heat transfer enhancement in solar air heater duct which was installed with conical protrusion array by Alam and Kim [8]. In their study, four relative protrusion height and four relative rib pitch under the four Reynolds number of 4,000 - 16,000. The thermal efficiency was increased when Reynolds number increased in both different protrusion height and pitch. Moreover, they compared their conical protruded surface with spherical protruded surface. The result showed that the Nusselt number of conical protruded surface was higher than spherical one.

In according with above mentioned research, the study of different model of dimple and protrusions can affect on heat transfer and flow characteristics. Some researcher showed the heat transfer enhancement for teardrop protrusion/dimple are higher than spherical dimple/protrusion.

Therefore, the teardrop dimple /protrusion with constant eccentricities was researched experimentally and numerically in this study. The aim of this study was to show that the effect of different spacing of dimple-to-dimple and protrusion-to protrusion of teardrop model can affect the heat transfer and flow characteristics.

2. Methodology

2.1 Apparatus of Experiment

Experiments have been performed to analyse heat transfer characteristics over the protruded teardrop surface of wind tunnel. The schematic of wind tunnel set up is shown in Figure 1. The rectangular wind tunnel was assembled with air by a 3-HP blower which was controlled by adaptable frequency related to Reynolds number. The air was passed through the 2-KW heater for heating up to control the temperature $T_{inlet}=25.7^{\circ}\text{C}$ which was adjusted by power controller. The flow straighteners were assembled at the inlet and, the mesh plate was used after the flow straighteners to prevent the unnecessary particles which disturb the air flow. The rectangular cross section wind tunnel which was configured with 300 mm in width, 26.4 mm in height and 2,450 mm in length was connected after the mesh plate section. The wind tunnel was composed of three sections, i.e., the test section, upstream and downstream test section. The downstream test section was having 490 mm in length related to blower. The upstream test section was 1700 mm in length related to mesh plate, flow straightener and heater. The test section which was installed teardrop protrusion inline arrangement was 280 mm in length. The bottom surface of the test section was drilled with rectangular hollow and covered with stainless-steel foil having 0.03mm in thickness. The TLC sheet was attached on the stainless-steel foil on the external side. This stainless-steel foil was stretched between copper bus bars. The foil was supplied with the required electrical power through these copper bus bars using DC power source which can be adjusted to a different current and voltage. The TLC sheet was attached on the stainless-steel foil. A digital camera was used to capture the colour patterns of TLC sheet on the surface by converting images of colour pattern of TLC sheet, which was arranged at accurate scale size from red, green, and blue (RGB) system to a hue, saturation, and intensity (HSI) system. The correlated temperature equation which was examined by the experiment result of TLC sheet temperature was used in MATLAB. The details of temperature calibration for TLC sheet were described in previous works of Wae-hayee *et al.* [9, 10].

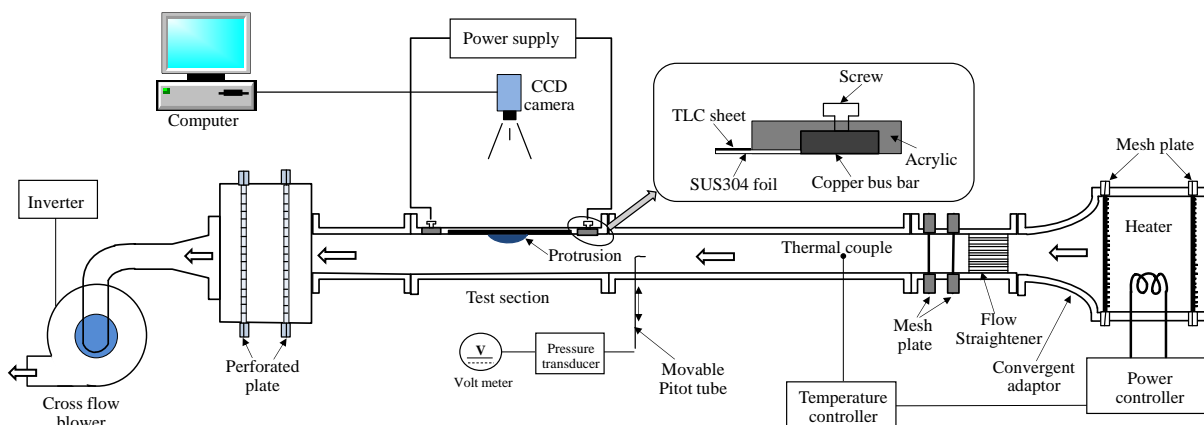


Fig. 1. Schematic diagram of experimental set-up for teardrop protruded channel

2.1.1 Model of study

The experiments have done on the heat transfer with five protrusions of teardrop with negative and positive eccentricity which were installed over the test section of wind tunnel as shown in Figure 2. Due to the limitation of experimental set up, only the protrusion cases were studied in the experiment. The sketches of teardrop protrusions and dimples with different eccentricities such as PE and NE are shown in Figure 3 and 4. The figure clearly shows the position of teardrop protrusions over the test section which was designed to get enough fully developed flow and the coordinating system. The X, Y and Z coordinates which are located at the centre of middle protrusion/dimple show flow direction, direction of wind tunnel height and perpendicular direction to the flow. The printed diameter of concave of teardrop was $D=26.4$ mm and the height of teardrop protrusion or the depth of teardrop dimple was $H=5.28$ mm. The spacing of protrusion-to-protrusion and dimple-to-dimple was varied with four cases i.e., $S/D= 1.125, 1.25, 1.5$ and 2 . In this study, the Reynolds number was considered base on hydraulic diameter of wind tunnel $Re_H=20,000$ [11, 12 and 18].

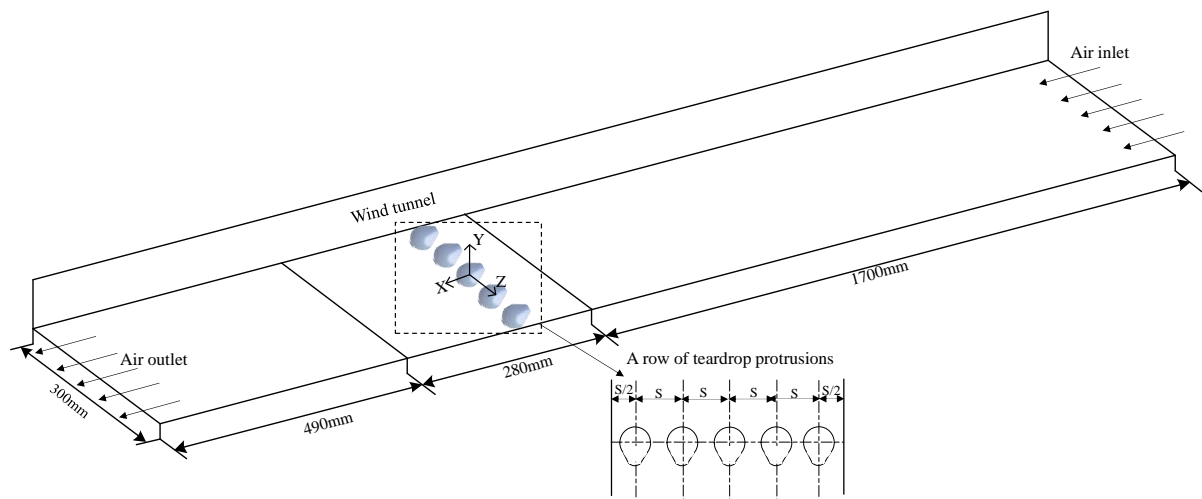


Fig. 2. Diagram of teardrop protrusion location in the wind tunnel

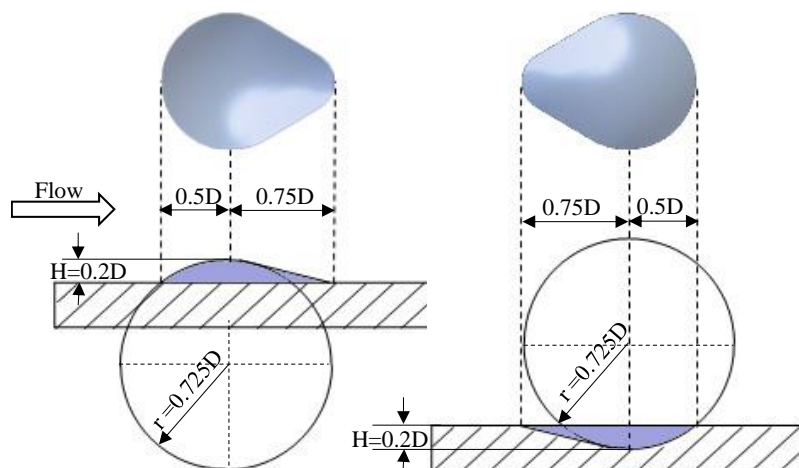


Fig. 3. Geometrical parameter of teardrop dimple and protrusion

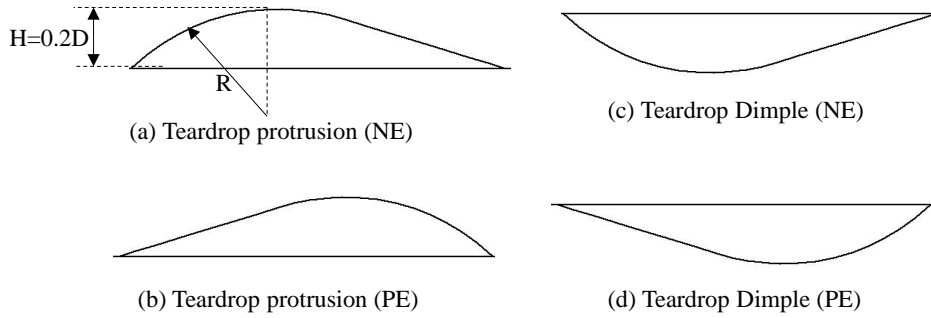


Fig. 4. Teardrop protrusion and dimple with different eccentricities

2.2 Heat Transfer Measurement

The coefficient of local heat transfer by force convection of heated test section surface was calculated from:

$$h = \frac{\dot{q}_{input} - \dot{q}_{losses,convection} - \dot{q}_{losses,radiation}}{A(T_w - T_a)} \quad (1)$$

Where, T_w is wall temperature and T_a is temperature of entering air into wind tunnel.

The heat flux generation on the test section surface can be calculated from:

$$\dot{q}_{input} = \frac{I^2 \cdot R}{A} \quad (2)$$

Where, I is the current of supplied electrical current, R is the electrical resistance of stainless-steel foil and A is the area of heat transfer surface.

The convection and radiation heat loss from TLC sheet to environment were evaluated from:

$$\dot{q}_{loss,convection} = h_c(\bar{T}_w - T_s) \quad (3)$$

$$\dot{q}_{loss,radiation} = \sigma \varepsilon_{TLC} (\bar{T}_w^4 - T_s^4) \quad (4)$$

Where, h_c is the natural heat transfer coefficient from horizontal surface to surrounding obtaining from empirical equation, \bar{T}_w is average wall temperature and T_s is surrounding temperature. σ is the Stefan-Boltzman constant and ε_{TLC} is the emissivity coefficient of TLC sheet (=0.9).

The Nusselt number is defined as:

$$Nu = h \times \frac{D_H}{k} \quad (5)$$

Here, D_H and k are the tunnel hydraulic diameter and the thermal conductivity of the air.

The friction factor is obtained as follow:

$$f = \frac{P_1 - P_2}{1/2 \rho u^2} \times \frac{D_h}{L} \quad (6)$$

where P_1 and P_2 are pressure of inlet point 1 and pressure of outlet point 2. Moreover, u and ρ are the mean velocity of inlet air and density of air.

To calculate thermal performance, Dittus-Boelter correlation of Nusselt number for smooth surface of wind tunnel was used for fully developed turbulent flow.

$$Nu_0 = 0.023Re^{0.8} Pr^{0.4} \quad (7)$$

where Re and Pr are Reynolds number and Prandtl number of inlet air temperature.

The Blasius correlation equation is used for the friction factor of smooth surface of wind tunnel:

$$f_0 = 0.316Re^{-0.25} \quad (8)$$

The thermal performance, which is the main objective of this study is evaluated as follow:

$$\eta = \frac{(Nu / Nu_0)}{(f / f_0)^{1/3}} \quad (9)$$

2.3 Numerical Simulation

The three dimensional and steady state numerical simulation have done on the heat transfer and flow characteristics of teardrop dimpled/protruded surface of test section. The descriptions of boundary conditions for simulation are shown in Figure 5. The boundary condition and dimensions of numerical and experimental model are identical. The internal fluid flow was assumed as incompressible flow with constant thermal properties. All walls were insulated and assumed as an adiabatic condition except for the bottom wall of the test section which was treated as heat transfer surface. The tunnel's top and bottom walls were specified as no-slip boundary condition. For reducing computational efforts, the lateral sides of the wind tunnel were given as symmetry condition remaining with three middle protrusions. Therefore, the width of tunnel was varied with the different protrusion-to-protrusion/dimple-to-dimple spacing (S). The ratio of protrusion-to-protrusion/dimple-to-dimple spacing to printed diameter (S/D) was 1.125, 1.25, 1.5 and 2. The heat flux of the test section was set at 150 W/m² which was the same rage using in the experiment. The inlet of wind tunnel was considered as velocity inlet. The uniform velocity of inlet air was 6.44 m/s which was calculated according to the Reynolds number. The air was entered with uniform temperature of 25.7°C which is chosen according to experimental condition, and the pressure outlet boundary condition was used at the outlet of tunnel.

The computations for the flow and heat transfer in the dimpled/protruded channel were accomplished using ANSYS Fluent 15 software. The standard k- ω SST turbulence model was used in numerical simulation. According to the Shen et al. [13] and Wright et al. [14], they compared their experimental result of Nusselt number with SST k- ω , k- ω , RNG k- ω and realizable k- ω models. They described that the data which was using SST k- ω model matched well with experimental data and this model is very suitable for dimple/protrusion structure. Therefore, SST k- ω turbulence model was used because this model was good for detecting flow structures and reducing computation cost [15, 16 and 17]. Moreover, a second order upwind spatial discretization method was applied for momentum equation and turbulent capacity to decrease the computational error. In

the terms of convergence criteria, the root mean square (RMS) residual of continuity and energy equations were set to be minimum at 10^{-8} and that of momentum equation was set to be minimum at 10^{-5} [18, 9 and 10].

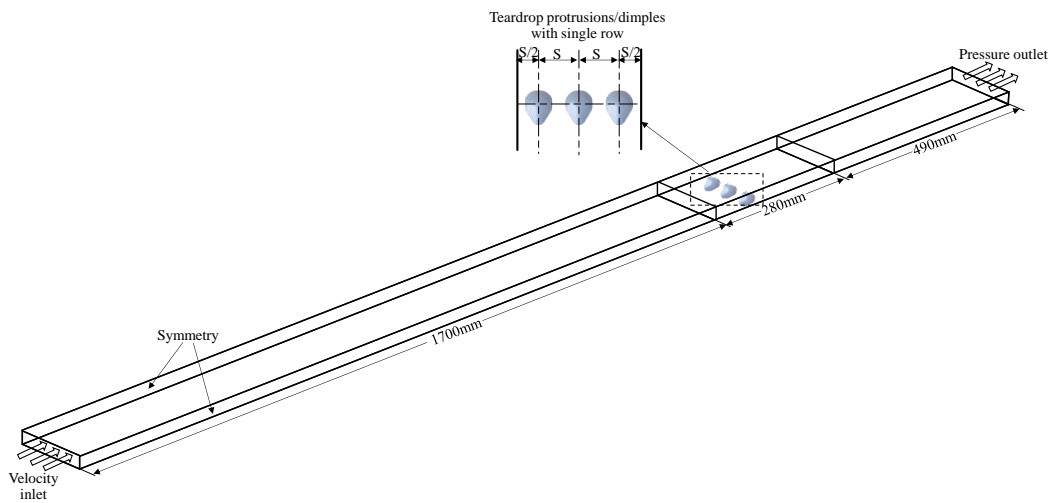


Fig. 5. The schematic of boundary conditions for wind tunnel simulation

The details of generated grid for computational model are illustrated in Figure 6. In this Figure, the details of internal grid system were described the spanwise cutting plane along the centre of protrusion/dimple and different view of protruded surface. For all simulation cases, even hexahedral meshes were applied for simulation model of wind tunnel, but uneven hexahedral meshes were applied for the non-uniform surface of protruded area as well as border of protruded regions. The grid system which was used in this study was examined by providing the y^+ value being lower than one [13, 19]. The grid numbers were saturated with various grid scale system for simulation which was considered within the range of 1.8 to 7.7 million elements, and 7.2 million elements were selected to use in computation domain.

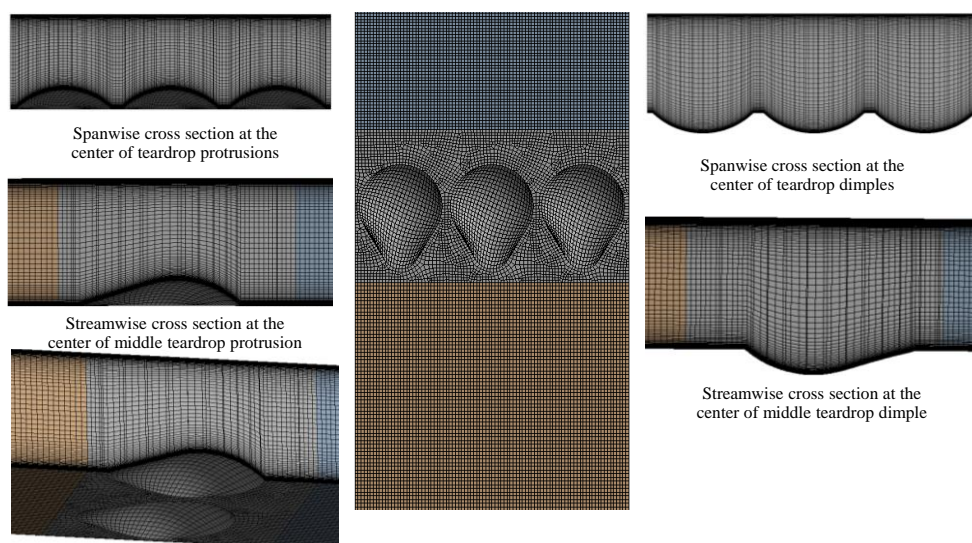


Fig. 6. The generated mesh for teardrop dimple/protrusion computation

3. Results and Discussion

3.1 Flow Characteristics

The streamline flow conditions at the centre of middle teardrop dimples/protrusions for $S=1.125D$ case are shown in Figure 7. The flow starts separation when the flow enters to the dimple cavity. Inside the dimple, the recirculation flow which can reduce heat transfer. Some upstream flow moves toward to the downstream above these circulation regions, which can cause significant reattachment flow. The fluid flows smoothly into the teardrop dimple (PE) and the vortex structure was happened at the downstream half of dimple cavity. Compare with these two dimpled cases, the reattachment flow region or length for teardrop dimple (NE) was larger or longer than that for teardrop dimple (PE). Inside the dimple cavity, the unsymmetrical vortex flow was occurred in teardrop dimple (PE) case.

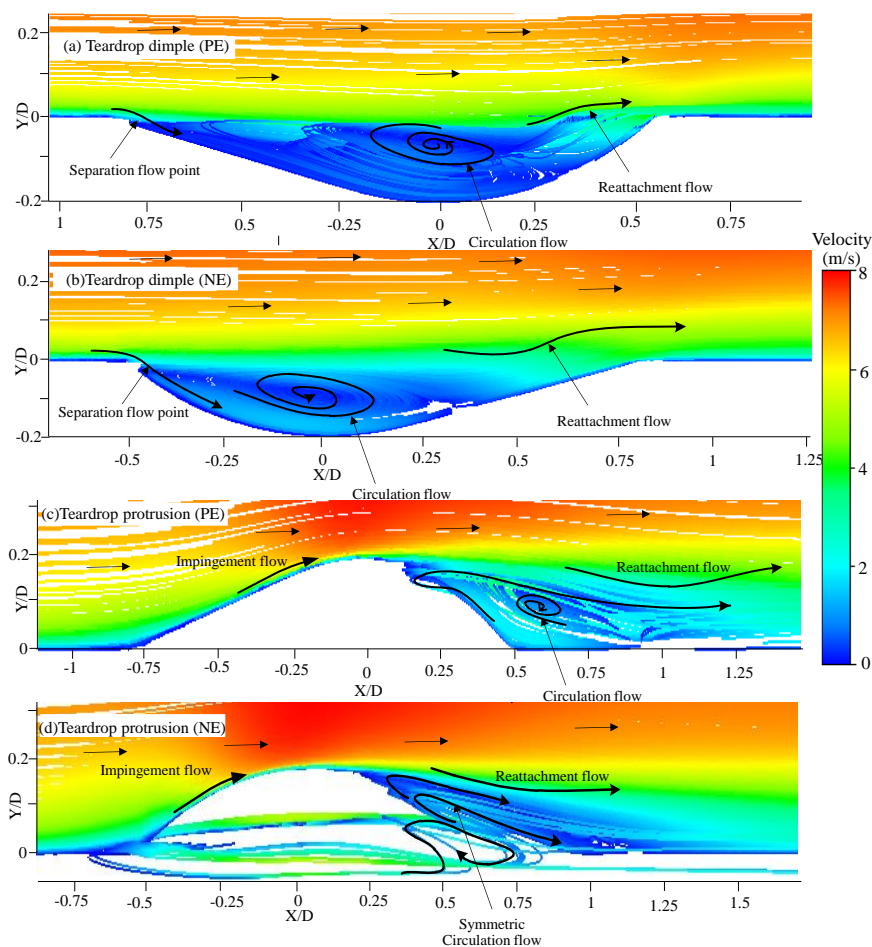


Fig. 7. Streamline at the centre of teardrop dimples/protrusions for $S=1.125D$ (Simulation results, $Re_H=20,000$)

For teardrop protrusion (PE), the fluid flows smoothly over the protrusion and some flows move along with the edge of both sides of protrusion to the downstream of protrusion. Therefore, the symmetrical vortex pair was occurred at the downstream region of protrusion. The reattachment flow was found over these symmetrical vortexes. It can be clearly seen in Figure 7(c). For teardrop protrusion (NE), the separation flow was found near the front edge of protrusion. Some of fluid flows

along with the edge of protrusion to the trailing edge of downstream half of protrusion where the low-pressure region was occurred. Therefore, the separation flow was occurred at the trailing edge of protrusion and the reattachment flow was happened over these vortex pair at the same location. Comparing with those two figures, the symmetrical vortex condition for teardrop protrusion (PE) is stronger than that for teardrop protrusion (NE). And the region or length of reattachment flow for teardrop protrusion (PE) is larger than that for teardrop protrusion (NE).

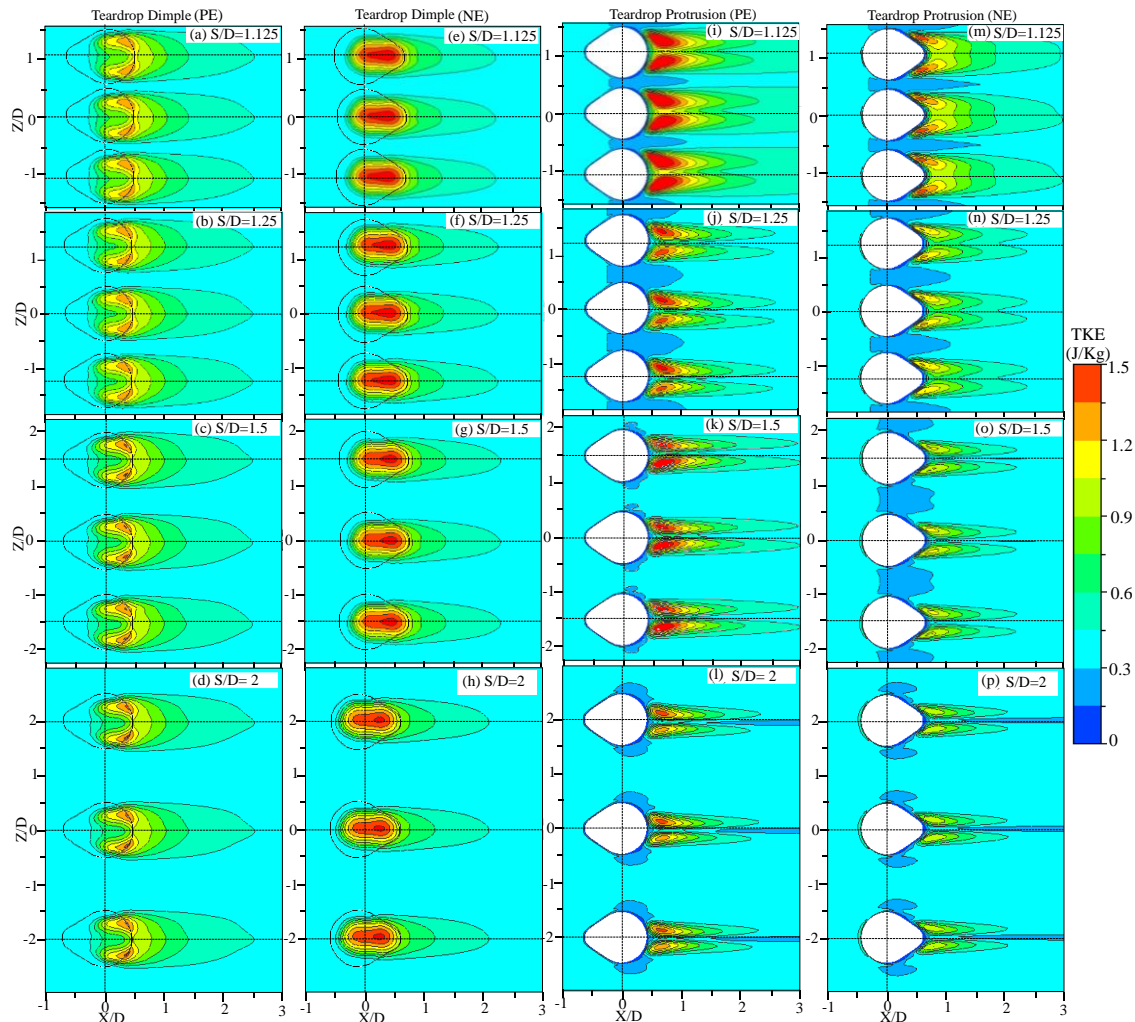


Fig. 8. Turbulence Kinetic Energy (TKE) contours above 1mm over the dimpled/protruded test section surface (Simulation results, $Re_H = 20,000$)

The simulation results of Turbulent Kinetic Energy (TKE) contours above 1mm over the dimpled/protruded surface are shown in Figure 8. The region of high TKE was occurred at the same location where the circulation or separation flow was occurred. The high TKE region of teardrop dimple (NE) is larger than that of teardrop dimple (PE) because the circulation flow inside the cavity of teardrop dimple (NE) is stronger than that of teardrop (PE). For teardrop dimple (PE), the flow enters easily inside the cavity and the symmetric vortex forms in both sides. Therefore, the symmetric contour of TKE was found in teardrop dimple (PE). Comparing all spacing case, the TKE region for $S=1.125D$ is larger than that for other cases. That is meant that the turbulence intensity for $S=1.125D$ case inside the dimpled cavity is stronger than that for others

In the teardrop protrusion cases, the high value of TKE was found behind the teardrop protrusion in both cases because the flow separation was occurred at this region. The high TKE area

for teardrop protrusion (PE) is larger than teardrop protrusion (NE) because the flow was blocked in front of teardrop protrusion (NE) and the small separation flow was occurred at the trailing edge of teardrop protrusion (NE). The detail of flow conditions was explained in figure. According to comparison of all spacing cases, the region of high TKE for $S=1.125D$ case was significantly larger than that for other cases because small spacing case causes the strong interaction of vortex pair between the spacing of protrusion-to-protrusion.

3.1 Heat Transfer Characteristics

The Figure 9 shows contour of Nusselt number distribution on the teardrop dimpled/protruded test section surface at $Re_H = 20,000$. The low Nusselt number region was occurred at the upstream half of dimpled cavity where circulation flow was found. The high Nusselt number area of teardrop dimple was found at just downstream of dimple. For teardrop dimple (PE), the reattachment flow region is lower than (NE) cases and the unsymmetrical vortex pair was occurred while symmetrical vortex pair was found in teardrop dimple (PE) case. Therefore, the area of high Nusselt number for teardrop dimple (NE) is higher than that for teardrop dimple (PE). Moreover, the two-peak region of Nusselt number distribution was found in teardrop dimple (NE) case while one peak region of Nusselt number distribution was found in teardrop dimple (PE). The high Nusselt number region becomes smaller when the spacing gets larger.

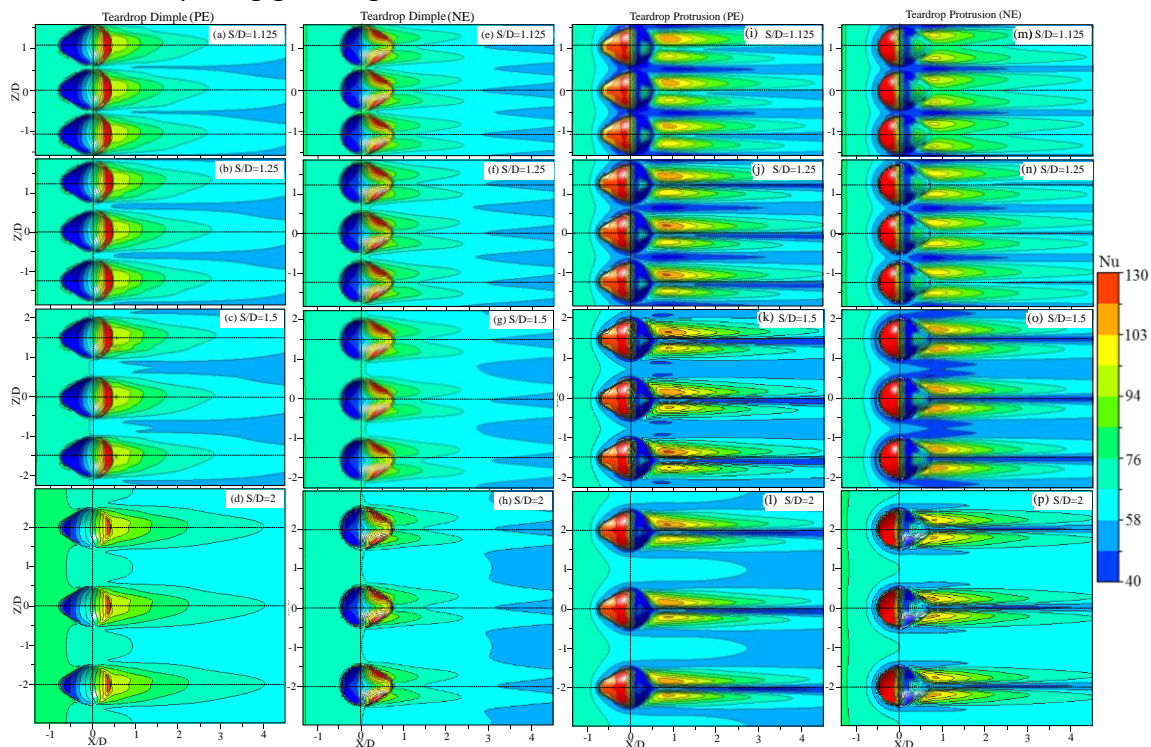


Fig. 9. Contour of Nusselt number distribution on the teardrop dimpled/protruded test section surface (Simulation results, $Re_H = 20,000$)

The high Nusselt number region was found at the upstream half of teardrop protrusion where the impingement flow was happened. For teardrop protrusion (PE), the fluid flows smoothly over the protrusion and the strong separation flow was occurred at the downstream half of protrusion. This effect can enhance heat transfer. However, the fluid was blocked at the upstream of teardrop protrusion (NE) and the vortex intensity at the trailing edge of protrusion was low because some fluid

flows both side of protrusion rim. Therefore, the Nusselt number region behind the protrusions for teardrop protrusion (PE) is higher than that for teardrop protrusion (NE)

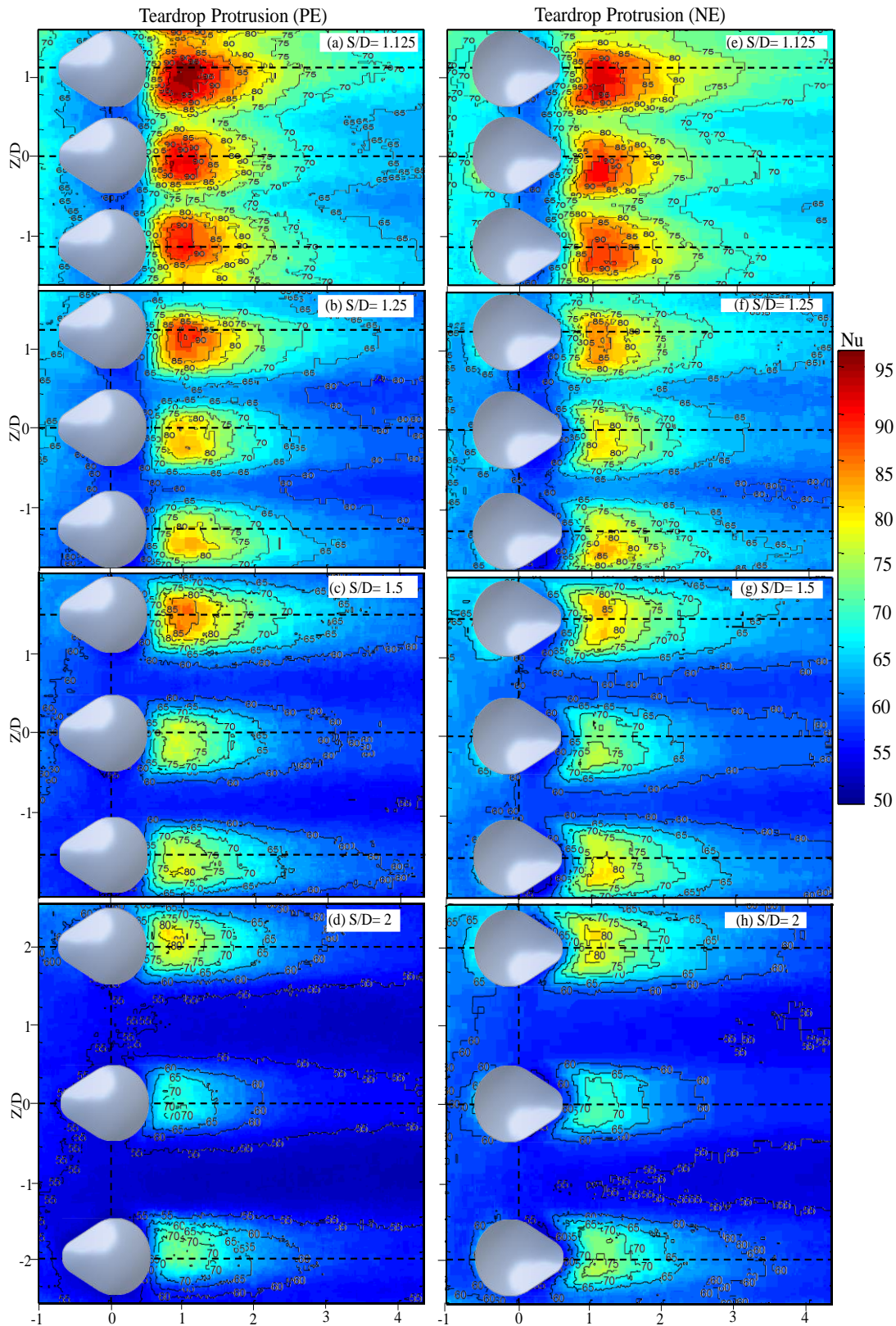


Fig. 10. Contour of Nusselt number distribution on the teardrop protruded test section surface (Experimental results, $Re_H = 20,000$)

The Figure 10 shows the experimental results for contour of Nusselt number distribution over the middle three protrusion of test section. This study was not considered for the area of teardrop protrusion surface. All experimental results were considered under the same range ($50 \leq Nu \leq 100$). In general, the high Nusselt number regions were occurred at the downstream of teardrop protrusion where the reattachment flow was found. The low Nusselt number region was happened just near the downstream rim of teardrop protrusion where the separation flow was occurred. And then, the high Nusselt number area became smaller when the spacing became narrower because of the interaction vortex pair between the spacing of protrusion-to-protrusion. Therefore, the narrowest case can cause the high TKE, high Nusselt number value and strong turbulence intensity. According to the comparison between teardrop protrusion (PE) and (NE), the Nusselt number region for teardrop protrusion (PE) is higher than that for teardrop protrusion (NE) case in every single-spacing case because the turbulence intensity of teardrop protrusion (PE) is stronger than that of NE case. These results can agree well with the simulation results of TKE for teardrop protrusion, which was discussed in flow characteristic section.

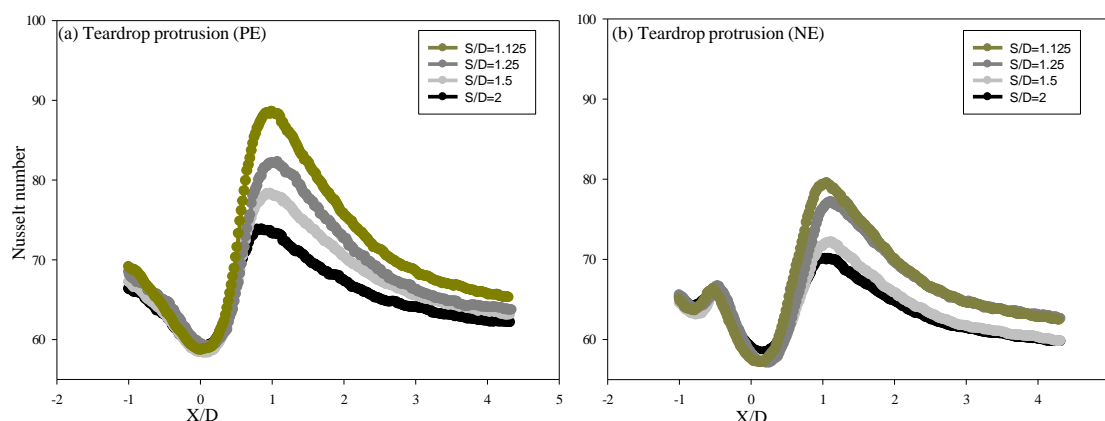


Fig. 11. Average Nusselt number trend along with the X/D direction of protruded test section surfaces (Experimental results, $Re_H = 20,000$)

The Figure 11 shows the average Nusselt number along with the streamline direction of protruded test section surfaces. For teardrop protrusion (PE), the fluid flows smoothly over the protrusion at the upstream of protrusion. Therefore, the Nusselt number values at the upstream of protrusion is normal. However, the flow was block at the upstream in the case of teardrop protrusion (NE). This condition can make small separation flow at there. Therefore, the Nusselt number value drop immediately at the upstream of protrusion where separation flow was occurred. The trend of average Nusselt number values was significantly high behind the teardrop protrusion where reattachment flow was found in both cases. It can be seen clearly that the values of teardrop protrusion (PE) were higher than that of teardrop protrusion (NE). The results of TKE and flow characteristics from simulation are quite match with experimental results.

The Figure 12 shows the Turbulence Kinetic Energy (TKE) distribution of simulation results at the centre of middle protrusions ($Z/D=0$). For teardrop protrusion (PE), the flow passed through smoothly over the protrusion. Therefore, TKE value was low at in front of protrusion ($-1.2 \leq X/D \leq -0.75$). However, the small separation flow was found at the front edge of teardrop protrusion (NE). Therefore, the value of TKE of teardrop protrusion (NE) was a little higher than that of PE case at the position of ($-1.2 \leq X/D \leq -0.75$). In general, the TKE value is high just behind the protrusion where the separation flow was occurred. The value of TKE for teardrop protrusion (PE) is higher than that of NE case in every single-spacing cases behind the protrusion. Among four spacing cases, the $S=1.125D$ case was significantly higher than other cases.

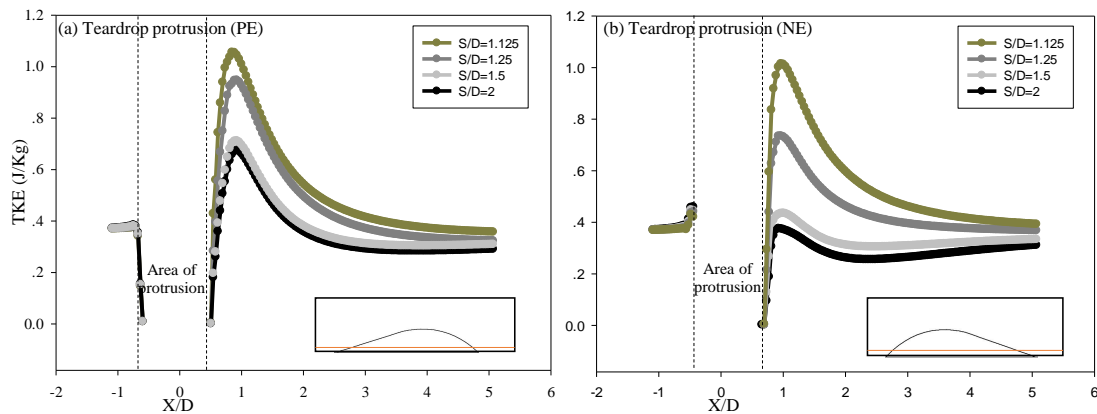


Fig. 12. Turbulence Kinetic Energy (TKE) distribution along X/D direction at the centre of middle protrusion above 1mm from the protruded test section surface

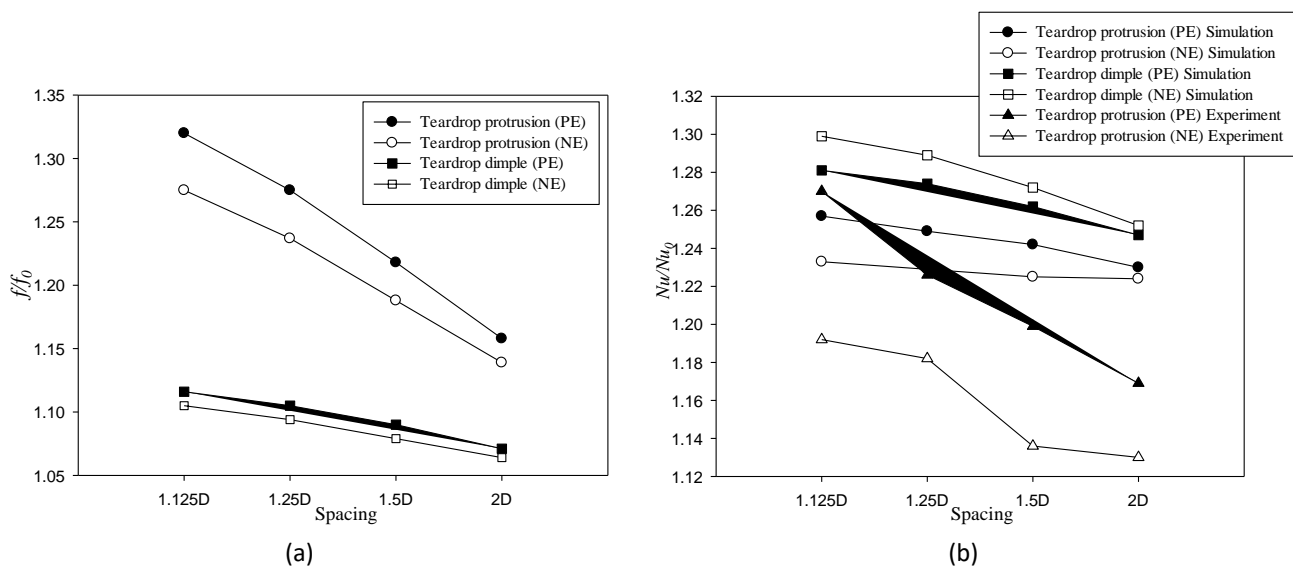


Fig. 13. (a) Friction factor of simulation result for teardrop dimple/protrusion ($Re_H = 20,000$) (b) Heat transfer enhancement of simulation result for teardrop dimple/protrusion ($Re_H = 20,000$)

The simulation results of friction factor for teardrop dimple/protrusion are shown in Figure 13 (a). In experiment, the pressure drop values of protruded test section surface is difficult to measure because this study was analysed single row of protrusions. According to the simulation results, the teardrop protruded surfaces are higher friction factor than dimpled surfaces because protrusions structure block the upstream flow. It can be noted that the friction factor value gradually decreases when the spacing increase. The narrowest spacing case was the highest friction factor because the pressure drop value is high in narrow spacing case. The friction factor of teardrop protrusion (PE) is higher than that of teardrop protrusion (NE) because of the different flow conditions which was discussed above session. Moreover, the friction factor of dimple (PE) is higher than that of (NE) case.

The Figure 13 (b) describes the heat transfer enhancement of simulation and experiment results of teardrop protruded/dimpled surface at $Re_H = 20,000$. In general, the heat transfer enhancement for teardrop dimpled surface was higher than that of protrusion cases because of different flow condition i.e. vortices generation, impingement flow, separation, recirculation and reattachment flow. The value of heat transfer enhancement in teardrop protrusion (PE) cases for both simulation and experiment are higher than that of NE cases. The teardrop protrusion (PE) of experiment for $S=1.125D$ case is 1.028% higher than that of simulation result. However, teardrop drop protrusion

(NE) of simulation for $S=1.125D$ case is 3.381% higher than that of experimental result. The values of heat transfer enhancement get low when the spacing becomes larger. The highest heat transfer enhancement case is teardrop dimple (NE) case.

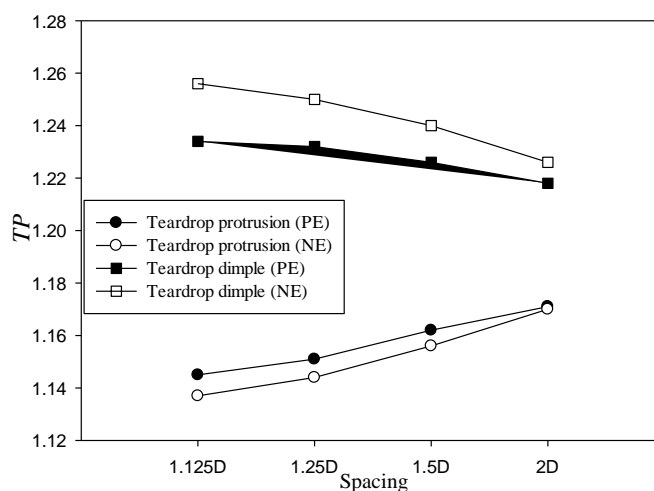


Fig. 14. Thermal performance of simulation result for teardrop dimple/protrusion ($Re_H=20,000$)

The thermal performance results of teardrop dimples/protrusions tested session surface for simulation are shown in Figure 14. The value of thermal performance for experimental results were not described because the friction factor cannot be calculated for the experimental analysis. The thermal performance for teardrop dimple case is higher than that for protrusion case. According to the comparison of protrusion cases, the thermal performance of teardrop protrusion (PE) is higher than that of teardrop protrusion (NE) due to high heat transfer enhancement in PE case. However, the thermal performance of teardrop dimple (NE) is higher than that of teardrop dimple (PE) case because of high heat transfer enhancement and low friction factor values in NE case. The thermal performance values for teardrop dimple are gradually decrease but the values for teardrop protrusion are gradually increase. For teardrop dimple case, the value of thermal performance for $S=1.125D$ case is the highest among four spacing cases because of highest heat transfer enhancement value and lowest friction factor value. The friction factor value in teardrop dimple case is very close comparing with four spacing cases. However, the thermal performance of teardrop protrusion case for $S=2D$ is the highest even though the value of heat transfer enhancement value is lowest. That is because friction factor value for $S=2D$ case is quite lower than that for $S=1.125D$ case.

4. Conclusions

The flow structures and heat transfer characteristics with different arrangements of teardrop dimples/protrusions in the rectangular wind were investigated. The conclusions of this study are as follow:

- i. The flow separation and recirculation inside the teardrop dimple (NE) is stronger than that of teardrop dimple (PE). Moreover, the symmetric vortex pairs are occurred strongly behind the teardrop protrusion (PE) while this flow is found at the trailing edge of teardrop protrusion (NE). Small separation flow is found at the upstream of teardrop protrusion (NE).
- ii. Among four spacing cases, the turbulent intensity for $S=1.125D$ is stronger than that for other cases because the effect of narrow spacing between protrusion-to-protrusion can cause

stronger separation flow and because of the effect of the longitudinal vortex flow along with the flow between the protrusion-to-protrusion spacing.

- iii. The heat transfer enhancement for teardrop dimple cases is higher than that for protrusion of simulation and experimental results. The values of teardrop protrusions (PE) are higher than that of teardrop protrusions (NE). However, the values teardrop dimples (NE) are higher than that of teardrop dimples (PE).
- iv. The highest values of average Nusselt number are occurred around the position of $X/D=1$ where the reattachment flow was found. Moreover, the position of the highest values of average Nusselt number is found identically where the position of highest TKE values was occurred.
- v. The thermal performance values for teardrop dimple cases decrease gradually while the values for teardrop protrusion cases increase gradually when the spacing become larger. That is because of the friction factor gap of spacing between each other's.

Acknowledgement

The research grant was supported by the Research and Development Office (RDO), Prince of Songkla University (PSU), grant No. ENG590725S and the scholarship award of Thailand Education Hub (THE-AC) from the graduate school of PSU.

References

- [1] Ligrani, Phill M, and Mauro M Oliverira. "Comparison of heat transfer augmentation techniques." *AIAA Journal* 41, no. 3 (2003): 337-362.
<https://doi.org/10.2514/2.1964>
- [2] Chyu, M.K., and Y. Yu, H. Ding, J.P. Downs, and F.O. Soechting. "Concavity enhanced heat transfer in an internal cooling passage." *The American Society of Mechanical Engineering paper*, 97-GT-437, (1997): 1-7.
<https://doi.org/10.1115/97-GT-437>
- [3] Mahmood, G. I., M. L. Hill, D. L. Nelson, P. M. Ligrani, H.-K. Moon, and B. Glezer. "Local heat transfer and flow structure on and above a dimpled surface in a channel." *Journal of Turbomachinery* 123, no. 1 (2000): 115-123.
<https://doi.org/10.1115/1.1333694>
- [4] Ligrani, P.L., J. L. Harrison, G. I. Mahmmud, and M. L. Hill. "Flow structure due to dimple depressions on a channel surface" *Physics of Fluids* 13, no. 11 (2001): 3442-3451.
<https://doi.org/10.1063/1.1404139>
- [5] Xie, Yonghui, Huancheng Qu and Di Zhang. "Numerical investigation of flow and heat transfer in rectangular channel with teardrop dimple/protrusion." *International Journal of Heat and Mass Transfer* 84, (2015): 486-496.
<https://doi.org/10.1016/j.ijheatmasstransfer.2015.01.055>
- [6] Acharya, Sumanta, and Fuguo Zhou. "Experimental and computational study of heat/mass transfer and flow structure for four dimple shapes in a square internal passage." *Journal of Turbomachinery* 134, no. 6 (2012): 061028-1-13.
<https://doi.org/10.1115/1.4006315>
- [7] Rao, Yu, Yan Feng, Bo Li, and Bernhard Weigand. "Experimental and numerical study of Heat transfer and flow friction in channel with dimples of different shapes." *Journal of Heat Transfer* 137, no. 3 (2015): 031901-1-10.
<https://doi.org/10.1115/1.4029036>
- [8] Alam, Tabish, and Man-Hoe Kim. "Heat transfer enhancement in solar air heater duct with conical protrusion roughness ribs." *Applied Thermal Engineering* 126, (2017): 458-469.
<https://doi.org/10.1016/j.applthermaleng.2017.07.181>
- [9] Wae-hayee, Makatar, Perapong Tekasakul, Smith Eiamsa-ard, and Chayut Nuntadusit. "Effect of cross-flow velocity on flow and heat transfer characteristics of impinging jet with low jet-to-plate distance." *Journal of Mechanical Science and Technology* 28, no. 7 (2014): 2909-2917.
<https://doi.org/10.1007/s12206-014-0534-3>
- [10] Wae-hayee, Makatar, Perapong Tekasakul, Smith Eiamsa-ard, and Chayut Nuntadusit. "Flow and heat transfer characteristics of in-line impinging jets with cross-flow at short jet-to-plate distance." *Experimental Heat Transfer* 28, no. 6 (2015): 511-530.
<https://doi.org/10.1080/08916152.2014.913091>
- [11] Won, Se Youl, Qiang Zhang, and Phillip M. Ligrani. "Comparisons of flow structure above dimpled surface with different

- dimple depths in a channel." *Physics of Fluid* 17, (2005): 045105-1-9.
<https://doi.org/10.1063/1.1872073>
- [12] Kore, Sandeep S., Rupesh J. Yadav, and Narayan K. Sane. "Investigations of effect of dimple depth on heat transfer and fluid flow within rectangular channel." *Procedia Engineering* 127, (2015): 1110-1117.
<https://doi.org/10.1016/j.proeng.2015.11.473>
- [13] Shen, Zhongyan, Yonghui Xie, and Di Zhang. "Experimental and numerical study on heat transfer in trailing edge cooling passages with dimples/protrusions under the effect of side wall slot ejection." *International Journal of Heat and Mass Transfer* 92, (2016): 1218-1235.
<https://doi.org/10.1016/j.ijheatmasstransfer.2015.09.042>
- [14] Wright, Lesley M., and Amir S. Gohardani. "Effect of coolant ejection in rectangular and trapezoidal trailing edge cooling passages." *Journal of Thermophysics and Heat Transfer* 23, no. 2 (2009): 316-326.
<https://doi.org/10.2514/1.38426>
- [15] Versteeg, Henk Kaarle, and Weeratunge Malalasekera. (2007). Chapter 3 – *Turbulence and Its Modelling: An introduction to computational fluid dynamics, Second Edition*. Pearson Prentice Hall, Page 3-72 – 3-80.
- [16] Zuckerman, N. and N. Lior. "Jet Impingement heat transfer: physics, correlations, and numerical modeling." *Advance in Heat Transfer* 39, (2006): 565-630.
[https://doi.org/10.1016/S0065-2717\(06\)39006-5](https://doi.org/10.1016/S0065-2717(06)39006-5)
- [17] Gerasimov, A. (2006). *Modeling Turbulent Flows with FLUENT*, Europe, ANSYS, Inc.2006.
- [18] Rao, Yu and Bo Li, and Yan Feng. "Heat transfer of turbulent flow over surfaces with spherical dimples and teardrop dimples." *Experimental Thermal and Fluid Science* 61, (2015): 201-209.
<https://doi.org/10.1016/j.expthermflusci.2014.10.030>
- [19] Salim, Salim M. and S.C. Cheah. "Wall y^+ strategy for dealing with wall-bounded turbulent flows." *Proceeding of the International Multi Conference of Engineers and Computer Scientists 2*, (2009): 2165-2170.